Hindawi
Advances in Materials Science and Engineering
Volume 2018, Article ID 5219624, 17 pages
https://doi.org/10.1155/2018/5219624

Research Article

Discretization of the Water Uptake Process of Na-Montmorillonite Undergoing Atmospheric Stress: XRD Modeling Approach

Walid Oueslati and Mahdi Meftah

UR 05/13-01 Physique des Matériaux Lamellaires et Nano-Matériaux Hybrides (PMLNMH), Faculté des Sciences de Bizerte, Université de Carthage, 7021 Zarzouna, Tunisia

Correspondence should be addressed to Walid Oueslati; walidoueslati@ymail.com

Received 30 March 2018; Accepted 22 May 2018; Published 16 September 2018

Academic Editor: Donatella Termini

This work focuses on the water-montmorillonite interaction under variable atmospheric conditions in order to characterize the interlamellar space (IS) configuration for possible use in the context of geological barrier for radioactive and industrial waste confinement. Atmospheric stress is achieved by applying, for Na-rich montmorillonite, a water sorption/desorption constraint, created at the laboratory scale. This hydrological disturbance allows the "demolition" of the clay history and to highlight the clay hydrous performance. The structural analysis is achieved using modeling of XRD profiles, which allowed us to determine the optimal structural parameters describing the IS configuration along the c^* axis. During the "in situ" XRD analysis, a sorption/desorption cycle is envisaged by variation of the relative humidity rate (%RH) from the saturated condition (94 %RH) towards extremely dry ones (2-3 %RH). Qualitatively, a new hydration hysteresis behavior of the "stressed" sample appears. Structural analysis achieved before and after perturbation allowed us to identify, respectively, the homogeneous hydration states, the hydrous transition domains, and the hydration heterogeneity degree. This latter parameter is characterized, quantitatively, by variable relative abundances of mixed-layer structure (MLS) population discerned over a wide explored RH range. Using the optimum structural parameter, the water molecule distribution versus the applied hydrous strain was quantified.

1. Introduction

The use of the smectite clay, like montmorillonite, as an canister envelope or as plugs or rock grout, in the context of geological barrier for industrial and/or radioactive hazardous waste confinement constitutes a green solution for severe environmental problems. In this regard, montmorillonite will be exposed to several environmental constraints (temperature cycle, extremely saturated conditions, high water pressure, etc.). Under these conditions, the clay-sealing ability is influenced, and two different scenarios can take place: (1) the crystal lattices may undergo permanent changes resulting in a largely reduced swelling and gel-forming capacity, and (2) the microstructure may become temporarily or permanently altered, which affects the cation exchange process [1–7].

The crystal structure of smectite consists of two sheets of principally tetrahedral Si with minor Al sandwiched to the top and bottom of a layer of octahedrally coordinated cations, usually Al but with some Mg and Fe [8, 9]. Furthermore, isomorphic substitution causes internal negative charges in the lamellae. The negative charges are compensated by adsorption of ions near the external surfaces of the clay minerals.

The smectite group of clay minerals with 2 : 1 layer structure is able to expand and contract its structures while maintaining its crystallographic integrity. Expansion takes place as water or some polar molecules enter the interlayer space [10].

The layers expand because the exchangeable cations attract more water than the relatively small layer charge [11]. The swelling is characterized by a stepwise expansion of the layer-to-layer distance with increasing water activity. This expansion has been described by the incorporation of 1, 2, and 3 planes of interlayer H_2O molecules, leading to the well-known 1W (d_{001} = 11.6–12.9 Å), 2W (d_{001} = 14.9–15.7 Å), and

3W (d_{001} = 18–19 Å) hydration states, in addition to the dehydrated one, 0W (d_{001} = 9.6–10.2 Å) [12].

The swelling of montmorillonite in various liquid systems has been investigated by several authors. These studies have focused on many parameters that come into play during the chemical clay-environment interaction. Indeed, to evaluate the mechanisms causing changes in the soil structure, Kaya and Fang [13] show that the physicochemical properties (i.e., cation exchange capacity (CEC), zeta potential (ζ), surface charge density, pore-size distribution, and Atterberg limits) of kaolinite, bentonite, and a local soil as the dielectric constant of the pore fluid change, such that as the dielectric constant of the pore fluid approaches that of the soil, the repulsive and attractive forces diminish. Smectite hydration and interlayer structure have been widely studied from both experimental and computational methods, mainly using X-ray diffraction (XRD) and some theoretical methods [14–31]. The studies [20, 32] show that hydration of swelling clays increases their basal spacing stepwise. Dazas et al. [31] investigate, under near-saturated conditions, the interlayer structure model of trihydrated low-charge smectite by X-ray diffraction and Monte Carlo modeling method. Oueslati et al. [29] characterize, using quantitative XRD analysis, the effect of the chemical composition of the soil solution on the structural change of Na-montmorillonite materials. On the contrary [30, 33], they investigate the effect of an environmental constraint, created in situ by varying the relative humidity rate, on the cation exchange performance and the structural changes of Na-montmorillonite in contact with Cd^{2+}, Co^{2+}, Zn^{2+}, Ni^{2+}, and Ba^{2+} chloride solutions.

Within this scope, and in extension with earlier works, this study is aimed at quantifying using the XRD modeling approach, the effect of an in situ applied hydrous perturbation on the hydration behavior and the structural changes of the most used host material in the earlier studies (i.e., the Na-exchanged montmorillonite). The structural parameters were determined by quantitative XRD analysis using an indirect method based on the comparison of the experimental 00l reflections with those calculated from structural models. This investigation allowed us to determine, respectively, the nature, amounts, position, and organization of exchangeable cations in the interlamellar space, along the c^* axis.

2. Materials and Methods

2.1. Starting Materials. The dioctahedral smectite used in this work is a reference montmorillonite sample (SWy-2) from the Source Clays Repository of The Clay Minerals Society [34]. The host material is characterized by a half-cell structural formula as follows [35]:

$$\left(Si_{3.923}Al_{0.077}\right)\left(Al_{1.459}Ti^{4+}_{0.018}Fe^{3+}_{0.039}Fe^{2+}_{0.045}Mg^{2+}_{0.382}\right) O_{10}(OH)_2\left(Ca^{2+}_{0.177}Na^{+}_{0.027}\right) \quad (1)$$

This clay mineral represents a major octahedral charge and exhibits an extremely limited substitution in the tetrahedral sheets where the cation exchange capacity (CEC) is 101 meq/100 g [36]. In order to guarantee a maximum dispersion, a preliminary treatment for the host materials is performed. The Na-rich montmorillonite suspension is prepared according to a classical protocol [37]. The obtained sample is referred to as SWy-2-Na.

2.2. Hydrous Perturbation. In order to achieve an atmospheric constraint (i.e., desorption process), a starting material suspension is placed in a sand bath at 50°C for 24 h to ensure a complete drying process. This sample undergoes a second humectation route (sorption process) by excessive addition of water followed by a moderate agitation. These two steps are repeated 50 times to ensure the destruction of the sample hydration history which is a principal parameter affecting its probable long use in the context of geological barrier.

2.3. XRD Measurements. For all samples, oriented slides were prepared by drying at room temperature an aqueous clay suspension on glass slides. XRD patterns were then recorded using a Bruker D8 diffractometer equipped with an MHG Messtechnik humidity controller coupled to an Anton Paar CHC+ chamber. Experimental XRD patterns were registered every 3 %RH scale at the fixed relative humidity condition values. Intensities were measured with a SolXE Si(Li) solid-state detector (Baltic Scientific Instruments) for 4 s per 0.04° 2θ step over the 2–32° 2θ Cu-Kα angular range. The divergence slit, the two Soller slits, the antiscatter slits, and the resolution slits were 0.3°, 2.3°, 0.3°, and 0.1°, respectively.

The samples were kept at 23°C in the CHC+ chamber during the whole data collection. The samples were kept also under a constant flow of mixed dry/saturated air to maintain the desired relative humidity (RH) after an initial equilibration. RH was continuously monitored with a hygrometer located close to the sample. To carry out the adsorption cycle, the RH value extended from 4% to the almost saturated condition (94 %RH). The reverse cycle (i.e., desorption) is accomplished by varying the moisture values in the opposite direction starting the dehydration process from 94 %RH and decreasing towards extremely dry ones (4 %RH).

2.3.1. Semiquantitative XRD Investigation. The diffractometer installation is monitored by DIFFRACPlus software (Bruker AXS GmbH, Karlsruhe, Germany) which allowed the calculation of qualitative parameters such as the basal spacing d_{001} from the first-order (001) Bragg reflections; the FWHM (full width at the half maximum intensity for the 001 reflection) and the rationality of the reflection position (ξ) related to the 00l reflections [38]. The combination of semiquantitative parameters with the profile geometry description (i.e., symmetric and asymmetric X-ray peaks) provides preliminary information about the hydration state evolution all over the explored RH range.

2.3.2. Quantitative XRD Investigation. The XRD modeling method is widely used to quantify hydration properties of smectite as a function of relative humidity [12, 13, 24–30, 33, 39, 40]. This indirect method consists of adjusting the experimental patterns by fitting positions and profiles of the 00l reflections over the explored angular range. Theoretical XRD patterns are calculated using the algorithms developed

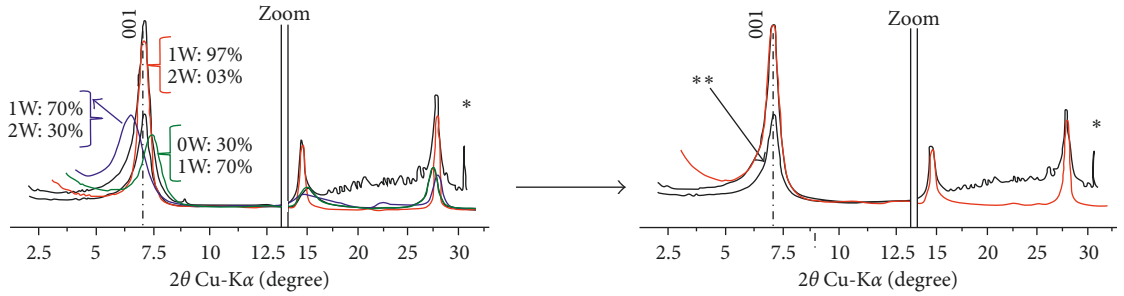

Figure 1: Example of an experimental XRD profile modeled using three MLSs containing (97%-1W, 3%-2W), (30%-0W, 70%-1W), and (70%-1W, 30%-2W), respectively. *Halite (NaCl) complex, **the 001 line is recorded twice time in order to check the sample balance with its environment.

in [41] and detailed later in [42]. The abundances of the diverse layer types (W_i), the mode of stacking of the different kinds of layers, and the mean number of layers per coherent scattering domain (CSD) are determined through XRD profile modeling. Within a CSD, the stacking of layers is described by a set of junction probability parameters (P_{ij}). The relationships between these probabilities and the abundances W_i of the different types of layers are given in [41]. All XRD profiles are simulated following the fitting strategy detailed in [24, 25], where the authors reproduce the experimental XRD pattern using various contributions to obtain a good fit, when it is not obtained with a unique periodic structure. Each contribution contains different layer types in variable proportions. However, the use of two or more mixed-layer structures to fit all features of experimental XRD patterns does not imply the actual presence of two or more populations of particles in the sample as discussed below. As a consequence, layers in the same hydration state as those present in the different mixed-layer structures must have identical properties at a given RH value. Each given layer type was thus assigned a unique chemical composition, a unique layer thickness value, and a unique set of atomic coordinates for all mixed-layer structures at a given RH. A detailed example of an experimental XRD profile modeled using three MLSs containing (97%-1W, 3%-2W), (30%-0W, 70%-1W), and (70%-1W, 30%-2W), respectively, is reported in Figure 1.

3. Results

3.1. Unstressed Sample

3.1.1. Qualitative XRD Analysis

(1) Sorption Process. For the starting materials, the evolution of the experimental XRD patterns versus %RH, reported in the Figure S1, shows a significant fluctuation of the position and intensity of the investigated 00*l* reflection along the hydration process. An additional reflection attributed to the Halite crystallization is present in up to 60 %RH. The qualitative investigation of the d_{001} value evolution, the FWHM, and the ξ parameters versus %RH (Figure 2) indicates heterogeneous hydration behavior for the transitional hydration state domain. This character is confirmed by the obtained high value of the cited parameters [29]. Based on this criterion, three principal transitional hydration domains along the sorption process can be reached and situated, respectively, between 10 and 34 %RH for 0W-1W, 49–67 %RH for 1W-2W, and 91–94 %RH for 2W-3W. For the three defined RH transition ranges, the XRD patterns are characterized by an asymmetric 001 reflection geometry accompanied by the corresponding high FWHM and ξ values (i.e., at 22 %RH, FWHM = 2.48° (2θ) and ξ = 1.84 Å; at 55 %RH, FWHM = 1.45° (2θ) and ξ = 1.58 Å; at 91 %RH, FWHM = 0.867° (2θ) and ξ = 1.13 Å), indicating probably an interstratified hydration character with more one layer type. Indeed, the d_{001} value shifts gradually from 0W (9.98 Å) towards 3W (18.86 Å) layer-type phase for the extreme %RH condition. The greatest clear 1W → 2W transition is observed from 52 %RH to 61 %RH. The 2W → 3W transition is observed from 85 %RH to 94 %RH.

(2) Desorption Process. The desorption sequence is achieved by decreasing the RH rate. The d_{001} basal spacing shifts from 18.86 Å, characteristic of a 3W hydration state (3W), to 9.96 Å, characteristic of a dehydrated state (0W). This evolution presents characteristic levels of almost homogeneous hydration states of hydration (3W, 2W, and 1W). Furthermore, there are transition regions 3W → 2W, 2W → 1W, and 1W → 0W, which are characterized by experimental profiles with an asymmetric diffraction line shape and an irrationality of the reflection positions, indicating probably a possible interstratified hydration state (Figure S2 and Figure 2). By comparing the widths (as a function of %RH) of the transition domains along the sorption and desorption processes (Figure 2), an offset is shown for 2W → 1W and 1W → 0W transitions.

Indeed, the 2W → 1W transition starts from 52 %RH and ends at 34 %RH, which is the RH value where the same transition ends during the sorption process. Similarly for the 1W → 0W transition, which starts from 13 %RH and ends at 4 %RH, there is a large offset to the hydration process whose 1W → 0W transition starts at 13 %RH and ends at 34 %RH.

This hydrous behavior shows the existence of hydration hysteresis reported in Figure 2. Also, during the desorption process, the absence of the pure dehydrated phase (0W), despite having reached the limit of 4 %RH, is noted.

In order to decode the insertion/disengagement mechanism of IS water molecules, this result can be explained by a freedom degree decrease for all the constituents inside the IS, which complicate the water molecule release process.

This fact can be interpreted by a transformation of the free water from the surrounding environment into structural

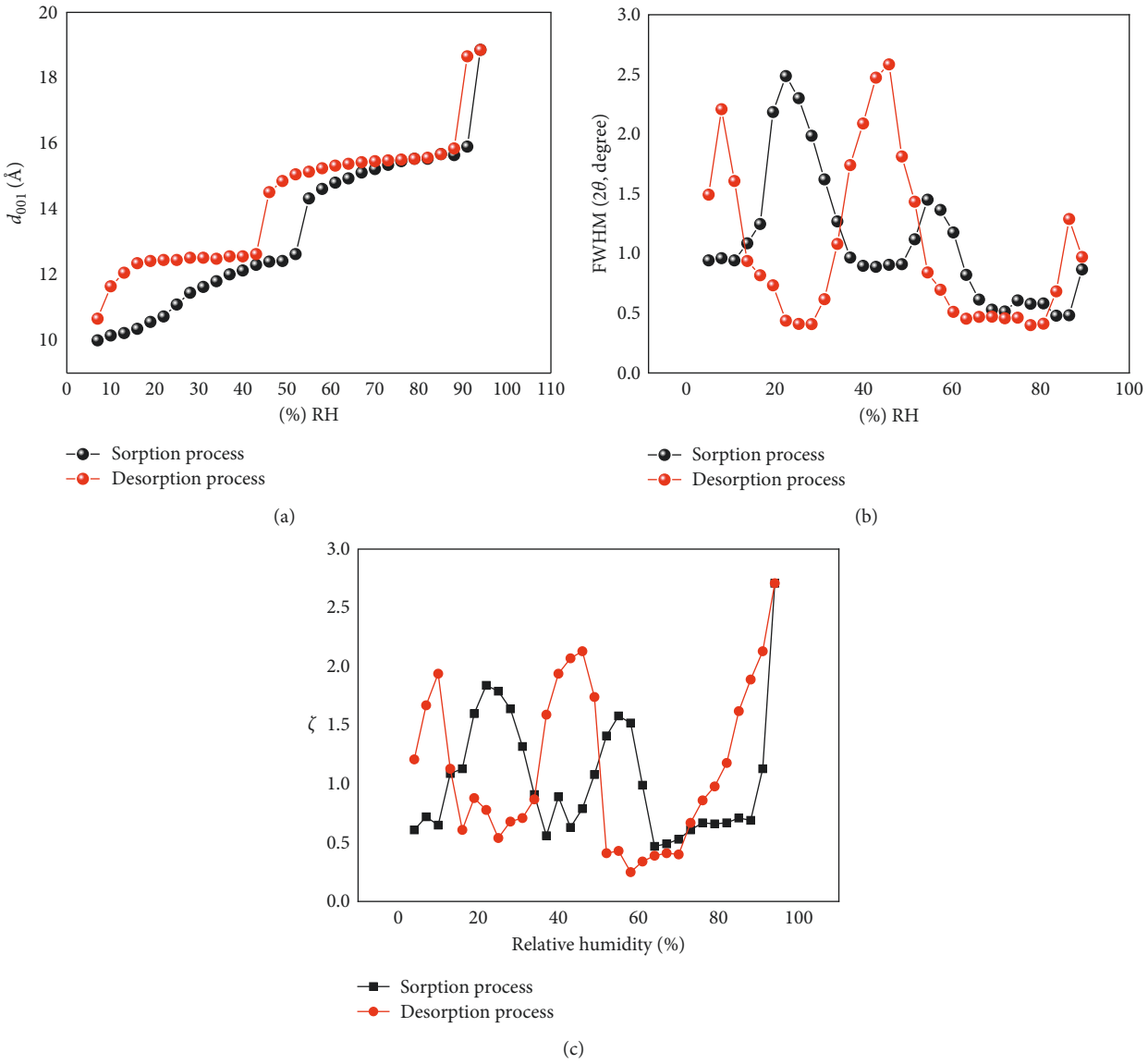

FIGURE 2: Evolution of the d_{001} (a), FWHM (b), and ξ parameters (c) versus %RH in the case of the unstressed sample along the sorption and desorption processes. The ξ parameter, which accounts for the departure from rationality of the $00l$ reflection series, is calculated as the standard deviation of the $l \times d_{00l}$ values calculated for the X_i measurable reflections ($X_i = 3$ in this case) over the 2θ Cu-Kα angular range (degree). Blue and yellow circles indicate interstratified hydration character (I) and homogeneous hydration character (H).

water, incorporated in the internal and external pore surfaces, which complicates its loss by dehydration.

The investigation of FWHM and ξ parameter shows the difference between the two processes for the transitions 2W → 1W and 1W → 0W (Figure 2). This problem does not arise for the 3W → 2W transition if we want to compare it with the 2W → 3W transition along the hydration process. Indeed, in this case, the high %RH value induces an elevated amount of water present in the IS; thereafter, the existence of a large fraction of water considered as "free water" will facilitate the process of dehydration.

3.1.2. Quantitative XRD Analysis

(1) Sorption Process. The hydration behavior obtained from the qualitative XRD analysis is refined by the quantitative analysis in order to quantify the clay "particle" composition.

The obtained best agreements between experimental and calculated intensity are reported in Figure S1, where a selection in the presentation was made in order to view areas with large fluctuations in the basal spacing value. All structural parameters used to fit experimental pattern are reported in Table 1 and Figure 3.

The distribution of water molecules in the theoretical model respects the results published in the literature [24, 29]. Indeed, for the 1W hydration state, one water sheet is located in the middle of the IS at the same position as the exchangeable cation. For the 2W hydration state, two water sheets are distributed on both sides of the middle of the IS. For the 3W hydration state, the exchangeable cation "bathes" in 3 water sheets superimposed along the c^* axis.

Table 1: Some structural parameters obtained from the quantitative XRD analysis in the case of the unstressed sample along the sorption process.

%RH	Layer stacking mode*	M
	R0	
4	—	7
	R0	
	R0	
7	—	7
	R0	
	R0	
10	—	8
	R0	
	R0	
	—	
13	R1 ($P_{AA} = 0.80$)	8
	R1 ($P_{AA} = 0.85$)	
	R0	
	—	
16	R1 ($P_{AA} = 0.85$)	8
	R1 ($P_{AA} = 0.70$)	
	R0	
	—	
19	R1 ($P_{AA} = 0.85$)	8
	R1 ($P_{AA} = 0.70$)	
	R1 ($P_{AA} = 0.75$)	
22	R1 ($P_{AA} = 0.70$)	8
	R0	
25	R1 ($P_{AA} = 0.75$)	9
28	R1 ($P_{AA} = 0.75$)	9
31	R1 ($P_{AA} = 0.75$)	7
34	R1 ($P_{AA} = 0.70$)	6
	R1 ($P_{AA} = 0.70$)	
37	R1 ($P_{AA} = 0.70$)	6
40	R1 ($P_{AA} = 0.70$)	5
43	R1 ($P_{AA} = 0.75$)	5
	R1 ($P_{AA} = 0.87$)	
46	R1 ($P_{AA} = 0.70$)	5
	R0	
	R1 ($P_{AA} = 0.87$)	
49	R1 ($P_{AA} = 0.70$)	5
	R0	
	R1 ($P_{AA} = 0.85$)	
	R1 ($P_{AA} = 0.96$)	
52	R1 ($P_{AA} = 0.70$)	5
	R1 ($P_{AA} = 0.70$)	
	R1 ($P_{AA} = 0.70$)	
55	R1 ($P_{AA} = 0.90$)	5
	R0	
	R1 ($P_{AA} = 0.70$)	
58	R1 ($P_{AA} = 0.90$)	6
	R1 ($P_{AA} = 0.75$)	
	R1 ($P_{AA} = 0.75$)	
61	R1 ($P_{AA} = 0.88$)	6
64	R1 ($P_{AA} = 0.75$)	5
67	R1 ($P_{AA} = 0.80$)	5
70	R1 ($P_{AA} = 0.85$)	5
73	R1 ($P_{AA} = 0.85$)	5
	—	
76	R0	5
	R0	
	—	
79	R0	5
	R0	
	—	
82	R0	5
	R0	
	—	
85	R0	7
	R0	
	R0	
88	R0	7
	R0	
	R0	
91	R0	7
	R0	
	R0	
94	R0	6

Note: 3W, 2W, 1W, and 0W are attributed to the layer hydration state. n_{H_2O}: the number of H_2O molecules per half unit cell is fixed to 2.5, 5.6, and 6.1, respectively, for 1W, 2W, and 3W. Z_{Na}: the position of exchangeable cations per half unit cell calculated along the c^* axis is fixed to 8.30 Å, 9.50 Å, 11.25 Å, and 12.60 Å, respectively, for 0W, 1W, 2W, and 3W hydration state. n_{Na}: the number of H_2O molecules per half unit cell is fixed to 0.33, indicating full saturation of the cation exchange capacity (CEC) of the minerals. *R, Reichweite factor; R0 and R1 describe the MLS with random interstratifications or with partial segregation; M: the average number of layers per particle; P_{AA}: layer succession law.

During the hydration process and for RH up to 43%, the experimental profile is reproduced by interstratification between the 0W and 1W phases with variable proportions, indicating the absence of a mono-homogeneous phase at 0W for humidity below 13 %RH (Figure 3).

On the contrary, an introduction of an R1 stacking mode type is noted at 13 %RH, which is consistent with the variation of the FWHM and ξ parameters. The first appearance of the 2W phase begins at 46 %RH and maintains a heterogeneous hydration state between 3 layer types (0W, 1W, and 2W) up to 58 %RH, where the structure is reproduced using a random distribution between the three mentioned phases. From 61 %RH, the contribution of the 0W phase disappears, and the experimental profile is completely reproduced by a combination of the 1W and 2W phases up to 76 %RH, where a minority phase related to the 3W hydration state is introduced. This combination continues up to 91 %RH, and then the 1W phase contribution disappears and the structure is completely modeled by 2W and 3W layer types. It should be noted that, at 94 % RH, the experimental diffractogram is reproduced by a majority 3W phase and the sample retains its interstratified character, which is in contradiction with the qualitative description mentioning a homogeneous phase. In contrast to the qualitative analysis, the quantitative analysis allowed us to show the existence of structural heterogeneities related to the coexistence of populations of several layers within the clay particle over the whole explored RH range.

(2) Desorption Process. For the desorption sequence and by decreasing humidity values up to 64 %RH, the experimental profile is modeled by a distribution of the two phases,

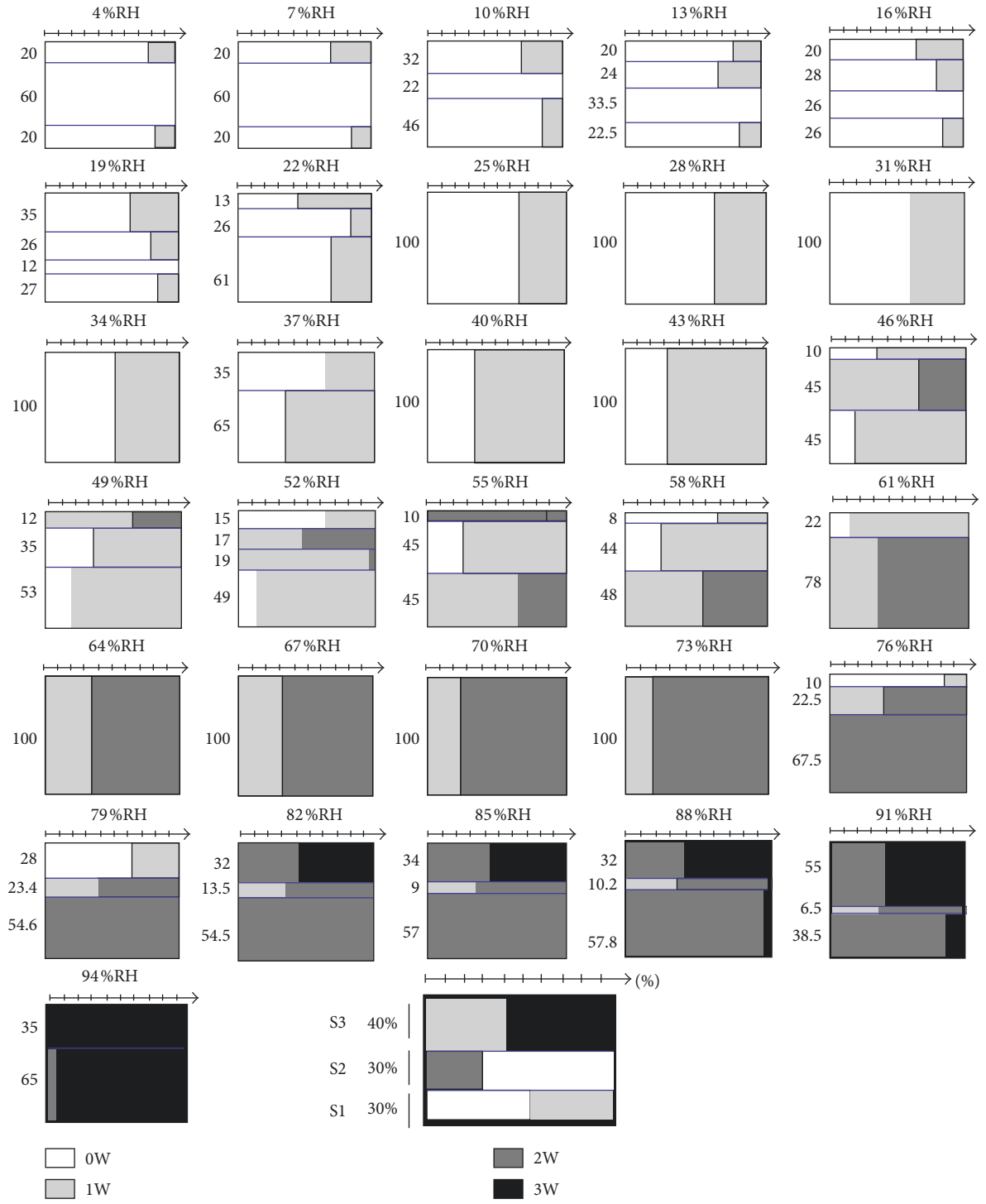

FIGURE 3: Schematic representation of the structure model used to fit the experimental XRD pattern in the case of the unstressed sample along the sorption process. Relative proportions, expressed in wt.%, of the three elementary mixed-layer structure (MLS) contributions are plotted on the *y*-axis, whereas their compositions (relative proportions of the different layer types) are plotted on the *x*-axis.

respectively, 3W and 2W. The basal distances and the proportions of the phase contributions used indicate a transition to the 2W hydration state. From 61 %RH and up to 58 % RH, the experimental profile is fully reproduced using segregated three phases mixed randomly. From 55 %RH and up to 34 %RH, the 3W phase disappears, which means a high retention of the water content, despite the relatively low RH and the absence of a sudden transition. At this humidity range, the structure is reproduced by a 2W/1W mixed structure. The first appearance of the 0W phase is obtained at 31 %RH, and its contribution in the theoretical model continues to increase as a function of the decrease in the RH rate. It should be noted that, for humidity ranging from 40 to 16 %RH, layers are stacked with random

Table 2: Some structural parameters obtained from the quantitative XRD analysis in the case of the unstressed sample along the desorption process.

%RH	Layer stacking mode	M
94	R0 R0	6
91	— —	3
88	R0 R1 ($P_{AA} = 0.80$)	4
85	R1 ($P_{AA} = 0.80$) R0	4
82	— R1 ($P_{AA} = 0.80$)	6
79	— R1 ($P_{AA} = 0.80$)	6
76	R1 ($P_{AA} = 0.86$) R0	6
73	— R1 ($P_{AA} = 0.86$)	6
70	— R1 ($P_{AA} = 0.92$)	6
67	— R1 ($P_{AA} = 0.86$)	6
64	— R1 ($P_{AA} = 0.96$)	7
61	— R1 ($P_{AA} = 0.96$) R0	7
58	R0 R1 ($P_{AA} = 0.96$) R0	7
55	R0 R1 ($P_{AA} = 0.96$)	7
52	R1 ($P_{AA} = 0.85$)	6
49	R1 ($P_{AA} = 0.88$)	6
46	R1 ($P_{AA} = 0.88$) R0	6
43	R1 ($P_{AA} = 0.88$) —	7
40	R0 R0	7
37	R0 R0	7
34	R0 R0	7
31	R0 R0 R0	7
28	— R0 R0	8
25	— R0 R0	8
22	— R0 R0	8
19	— R0 R0	8
16	R0 R0	8
13	R1 ($P_{AA} = 0.75$) R0	8
10	R1 ($P_{AA} = 0.50$) R1 ($P_{AA} = 0.55$)	8
7	R1 ($P_{AA} = 0.80$)	7
4	R1 ($P_{AA} = 0.89$)	8

distribution, and from 13 %RH, a partial tendency to segregation governs the stacking mode (Table 2 and Figure 4).

3.2. Stressed Sample

3.2.1. Qualitative XRD Description

(1) Sorption Process. From a macro point of view, the hydration behavior similar to that of the unstressed sample is observed in the case of the sample having undergone 50 drying/wetting cycles. Indeed, the d_{001} basal spacing value goes from 9.86 Å at 4 %RH relative to the 0W phase to 18.47 at 94 %RH, indicating a highly hydrated specimen (3W) (Figure S3). But the difference in behavior between the two hydration samples lies in the mechanism and the path followed during the swelling process. Indeed, for the stressed sample, the absence of homogeneous hydration levels characterized by homogeneous phases at 1W and 2W is noted. The evolution of experimental XRD patterns shows a 0W–2W transition over a wide range of humidity that starts at 16 %RH and ends at 70 %RH. This behavior is not observed in the case of the unstressed sample. The second difference is the absence of a homogeneous 3W phase for the maximum used RH values and the shift of the RH range for the homogeneous 2W phase. However, the hydration evolution versus %RH can be described by three main steps: (i) a logic starting from the 0W hydration state, (ii) a transition from 0W to 2W passing through an ephemeral 1W state, and (iii) an incomplete transition from 2W to 3W for high RH rates.

The exploitation of the calculated values of FWHM and ξ, reported in Figure 5, confirms the interstratified character observed during the 0W–2W and 2W–3W transitions. Indeed, a maximum of the FWHM value and ξ parameters is obtained for two ranges of humidity, respectively, that is, from 16% to 70 %RH and from 88% to 94 %RH. The homogeneous 0W and 2W hydration phases are characterized by low values of the abovementioned two parameters.

(2) Desorption Process. The evolution of experimental XRD patterns along the desorption process is shown in Figure S4. Along the explored RH range, a transition from an interstratified 3W hydration state to an interstratified 0W phase, characterized by an asymmetric 00l reflection with irrational positions, is observed (Figure 5). The followed dehydration way differs from that adopted during the hydration process indicating the appearance of a hydration hysteresis phenomenon. Depending on the RH value, during the dehydration

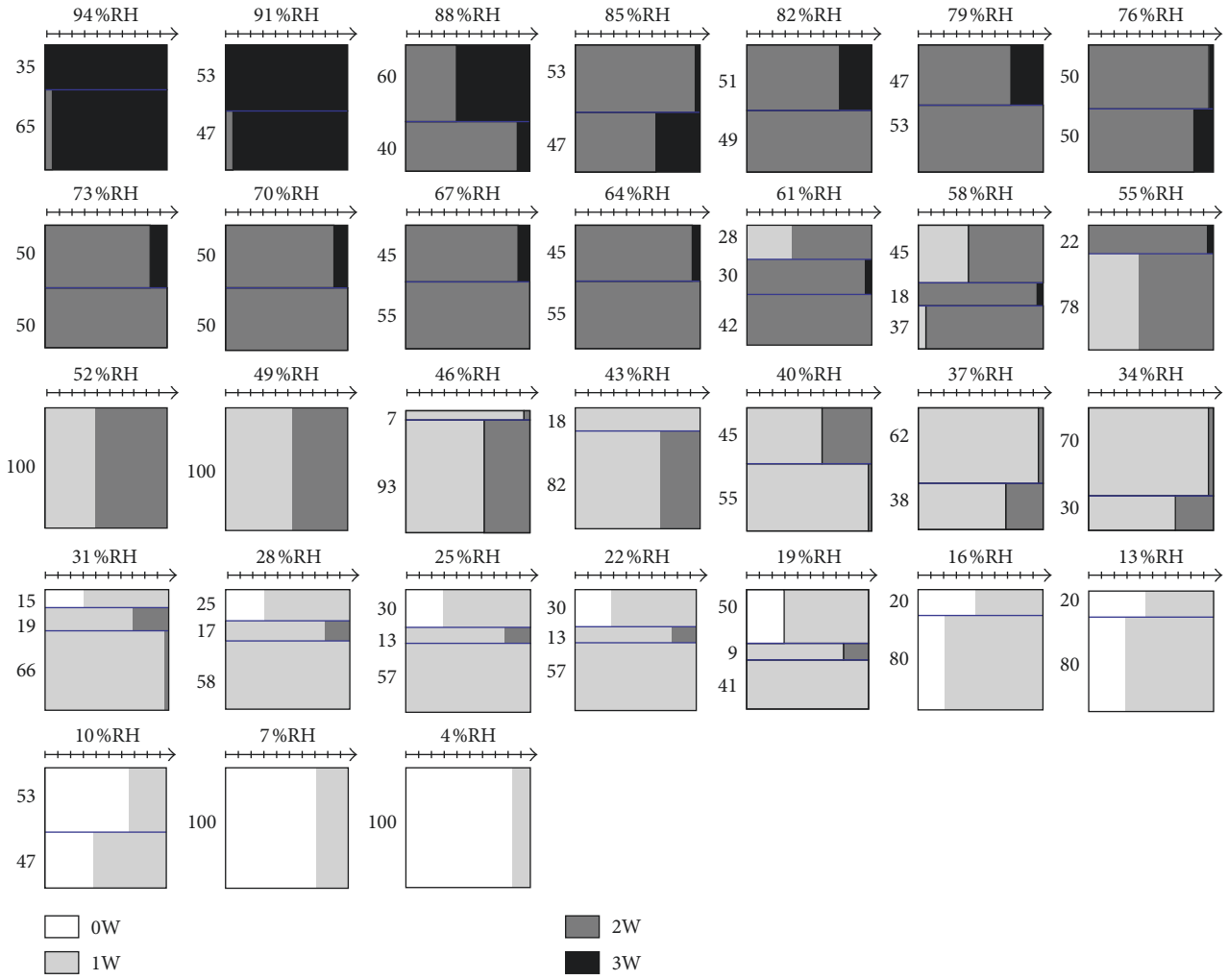

Figure 4: Schematic representation of the structure model used to fit the experimental XRD pattern in the case of the unstressed sample along the desorption process.

sequence, two hydration levels related, respectively, to the homogeneous phases 1W and 2W appear. The investigation of the FWHM and ξ parameters (Figure 5) allowed us to identify the interstratified type of the obtained phases during the dehydration process.

Indeed, from 91 %RH and up to 82 %RH, a fast 3W-2W transition with the absence of a purely trihydrated phase is observed. The homogeneous 2W phase begins at 79% and ends at 64 %RH. By comparing this result to that observed in the case of the "unstressed" sample, a decrease in the width of the RH range over which it is spreading is noted. This RH shift is probably attributed to an instability in the IS configuration or the easy release of the IS water molecule, due to RH value fluctuations. Indeed, from 61 %RH and up to 31 %RH, the evolution of the d_{001} basal spacing value indicates a slow progressive 2W-1W transition that can be interpreted as a small loss of interlayer water content. The 1W homogeneous state is observed over a very short RH range compared to the "unstressed" sample whose 1W level started at 31 %RH and reached 16 %RH. This result is consistent with the above, especially since a 1W-0W transition starts a bit early (from 23 %RH), which is not the case for the unstressed sample. The evolution of the different parameters from the qualitative analysis as a function of the %RH variation is reported in Figure 5. Several differences appear between the hydration and dehydration mechanisms obtained for the "stressed" sample. Whatever be the orientation of the hydration sequence and based on the low values of FWHM and ξ, only the homogeneous 2W state exists and a short and near-homogeneity is observed for the 1W state. On the contrary, an absence of the homogeneous 3W state, obtained in the case of the unstressed sample, is noted. The hysteresis effect (Figure 5) is present during both cycles, indicating a swelling behavior depending on the environmental conditions. The observed fluctuations, in terms of %RH width, the absence of homogeneous hydration domains, and characteristic phases of extreme RH conditions (4% and 94 %RH), confirm the major interstratified character observed for the "stressed" sample during the sorption/desorption sequence.

The evolution of the two parameters FWHM and ξ made it possible to determine a limit of homogeneity and/or heterogeneity of hydration and to confirm the geometric anomalies observed on the experimental XRD profiles.

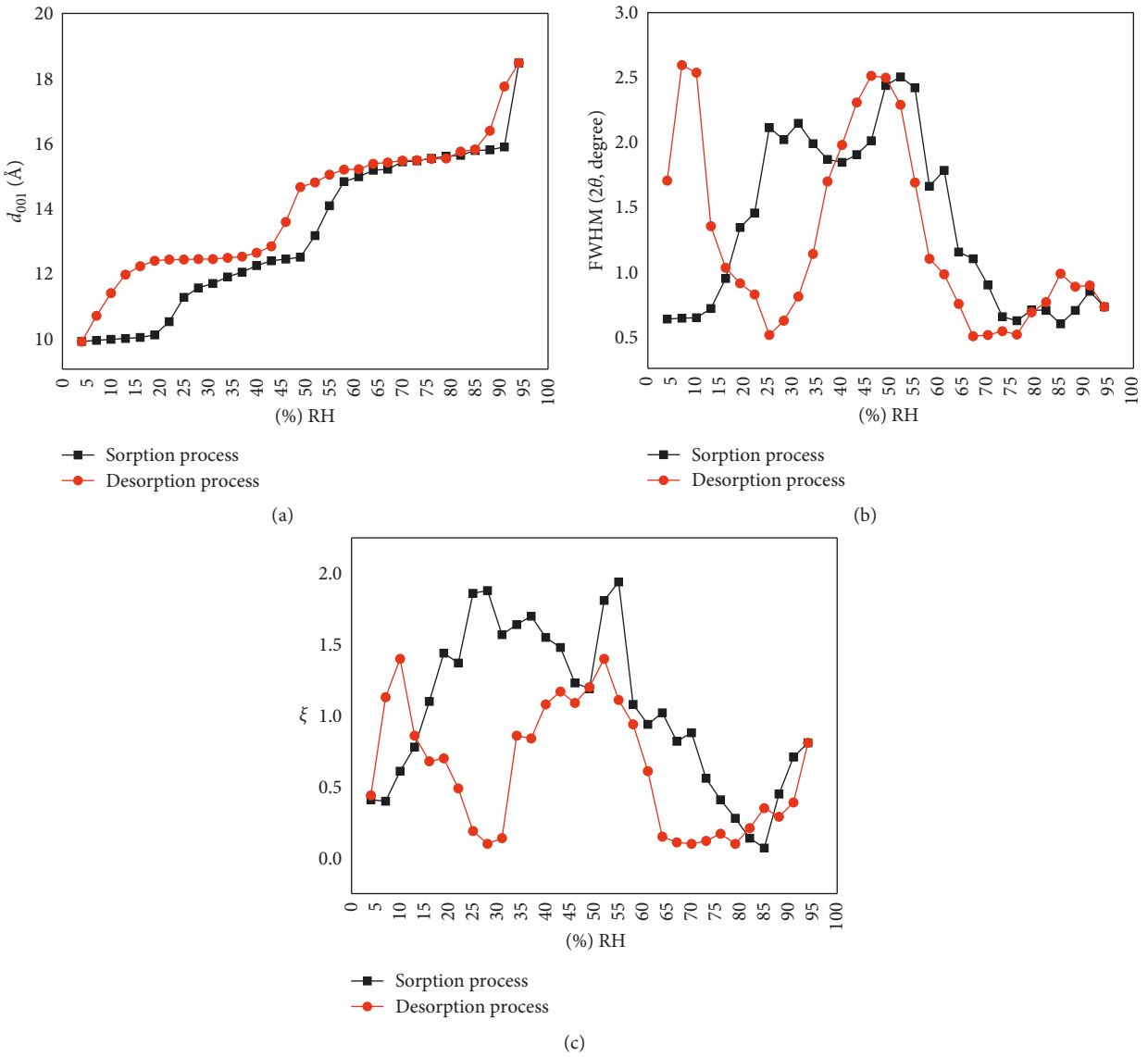

Figure 5: Evolution of the d_{001} (a), FWHM (b), and ξ parameters (c) versus %RH in the case of the stressed sample.

In general and for both sorption and desorption mechanisms, the "stressed" sample has more hydration heterogeneities than the "unstressed" sample. The interpretation of this result can be completed only after a quantitative analysis which makes it possible to quantify the abundances of the phases present in the structure and the contents of the IS.

3.2.2. Quantitative XRD Analysis

(1) Sorption Process. The obtained results deduced from the qualitative analysis are refined by quantitative analysis in order to quantify the composition of the clay "particle." All structural parameters used to model experimental XRD patterns are shown in Figure S3 and are summarized in Table 3 and Figure 6. Contrary to the results obtained during the qualitative analysis, concerning the homogeneous 0W and 2W hydration phases, the quantitative analysis shows the absence of any hydration homogeneities along the sorption process. In fact, for a humidity ranging from 4% to 37 %RH, the experimental profiles are reproduced by a 0W/1W mixture with variable abundances. The investigation of junction probabilities and the succession law between layers indicates a major segregation trend (R1). Also, qualitatively, the 2W transition starts at 52 %RH, which is not really the case since the introduction of a 2W layer "population" is done quantitatively at 40 %RH and the system (i.e., crystalline particle) is totally reproduced by 3 layer types (i.e., 0W, 1W, and 2W). This configuration does not exclude the 0W phase (which is in complete disagreement with the qualitative description), the contribution of which persists in the diffracted intensity, even for very high values of humidity. The three layer types are stacked with a segregation tendency.

At 34 %RH, the decrease of the average number of layers per half unit cell is due to hydration transition domain. This

Table 3: Some structural parameters obtained from the quantitative XRD analysis in the case of the stressed sample along the sorption process.

%RH	Layer stacking mode	M
	R0	
4	—	7
	R0	
	R1 ($P_{AA} = 0.90$)	
7	—	9
	R1 ($P_{AA} = 0.80$)	
	R1 ($P_{AA} = 0.90$)	
10	—	10
	R1 ($P_{AA} = 0.80$)	
	R1 ($P_{AA} = 0.90$)	
13	—	11
	R1 ($P_{AA} = 0.80$)	
	R1 ($P_{AA} = 0.90$)	
16	—	11
	R1 ($P_{AA} = 0.80$)	
19	R0	11
	R1 ($P_{AA} = 0.90$)	
	R1 ($P_{AA} = 0.80$)	
22	R1 ($P_{AA} = 0.90$)	11
	R1 ($P_{AA} = 0.70$)	
	R1 ($P_{AA} = 0.90$)	
25	R1 ($P_{AA} = 0.70$)	10
	R1 ($P_{AA} = 0.90$)	
28	R1 ($P_{AA} = 0.70$)	8
31	R1 ($P_{AA} = 0.70$)	8
34	R1 ($P_{AA} = 0.70$)	7
37	R1 ($P_{AA} = 0.70$)	7
	R1 ($P_{AA} = 0.70$)	
40	R0	7
	R1 ($P_{AA} = 0.75$)	
	R1 ($P_{AA} = 0.70$)	
43	R0	6
	R1 ($P_{AA} = 0.70$)	
46	R1 ($P_{AA} = 0.80$)	6
	R1 ($P_{AA} = 0.70$)	
49	R1 ($P_{AA} = 0.90$)	6
	R1 ($P_{AA} = 0.57$)	
	R1 ($P_{AA} = 0.70$)	
52	R1 ($P_{AA} = 0.90$)	6
	R1 ($P_{AA} = 0.57$)	
	R1 ($P_{AA} = 0.70$)	
55	R1 ($P_{AA} = 0.90$)	7
	R1 ($P_{AA} = 0.57$)	
	R1 ($P_{AA} = 0.70$)	
58	R1 ($P_{AA} = 0.90$)	6
	R1 ($P_{AA} = 0.60$)	
	R1 ($P_{AA} = 0.85$)	
61	R1 ($P_{AA} = 0.75$)	6
	R1 ($P_{AA} = 0.65$)	
	R1 ($P_{AA} = 0.85$)	
64	R1 ($P_{AA} = 0.75$)	6
	R1 ($P_{AA} = 0.68$)	
	R1 ($P_{AA} = 0.85$)	
67	R1 ($P_{AA} = 0.75$)	6
	R1 ($P_{AA} = 0.90$)	
	R1 ($P_{AA} = 0.85$)	
70	R1 ($P_{AA} = 0.75$)	6
	R1 ($P_{AA} = 0.90$)	
	R1 ($P_{AA} = 0.80$)	
73	R1 ($P_{AA} = 0.65$)	6
	R1 ($P_{AA} = 0.92$)	
	R1 ($P_{AA} = 0.95$)	
	—	
76	R1 ($P_{AA} = 0.92$)	6
	R1 ($P_{AA} = 0.85$)	
	R0	
79	—	6
	R1 ($P_{AA} = 0.85$)	
	R1 ($P_{AA} = 0.95$)	
82	R0	7
	R1 ($P_{AA} = 0.85$)	
	R0	
85	R0	7
	R1 ($P_{AA} = 0.85$)	
	R0	
88	R0	7
	R1 ($P_{AA} = 0.85$)	
	R1 ($P_{AA} = 0.93$)	
91	R0	6
	R0	
94	R1 ($P_{AA} = 0.85$)	6
	R1 ($P_{AA} = 0.97$)	

decrease in the M parameter is quantitatively reflected by diversity and a maximum number of MLSs present in the proposed theoretical model. The elevated heterogeneity degree is confirmed from 61 %RH, where the experimental profile is totally reproduced by 4 theoretical distributions (0W, 1W, 2W, and 3W). This combination of "population" is up to 76 %RH.

This result is probably due to a hard exfoliation mechanism of the IS under the effect of the constraint created by the drying/wetting stress.

From 79 %RH and up to 91 %RH, the 0W phase disappears and the system is reproduced by 3 phases only. At 94 %RH, the 1W phase disappears and the homogeneous 3W hydration state is never reached; however, the experimental profile is reproduced by a distribution between two phases (2W and 3W) stacked with a segregation tendency.

Physically, the existence of these hydration heterogeneities, in the quantitative analysis, agrees with the results of the qualitative analysis, indicating an increase in the values of FWHM and ξ on the same humidity range.

(2) Desorption Process. All structural parameters resulting from the quantitative analysis are summarized in Table 4 and Figure 7. In addition to the absence of the homogeneous hydration state over the entire explored RH range and contrary to the results of the qualitative analysis, the water molecule release is done in a progressive and continuous manner in the absence of any specific level. Indeed, from 94% up to 73 %RH, the experimental profiles are reproduced based on an arrangement of 2W and 3W phases stacked with a segregation tendency in the majority of cases. This result

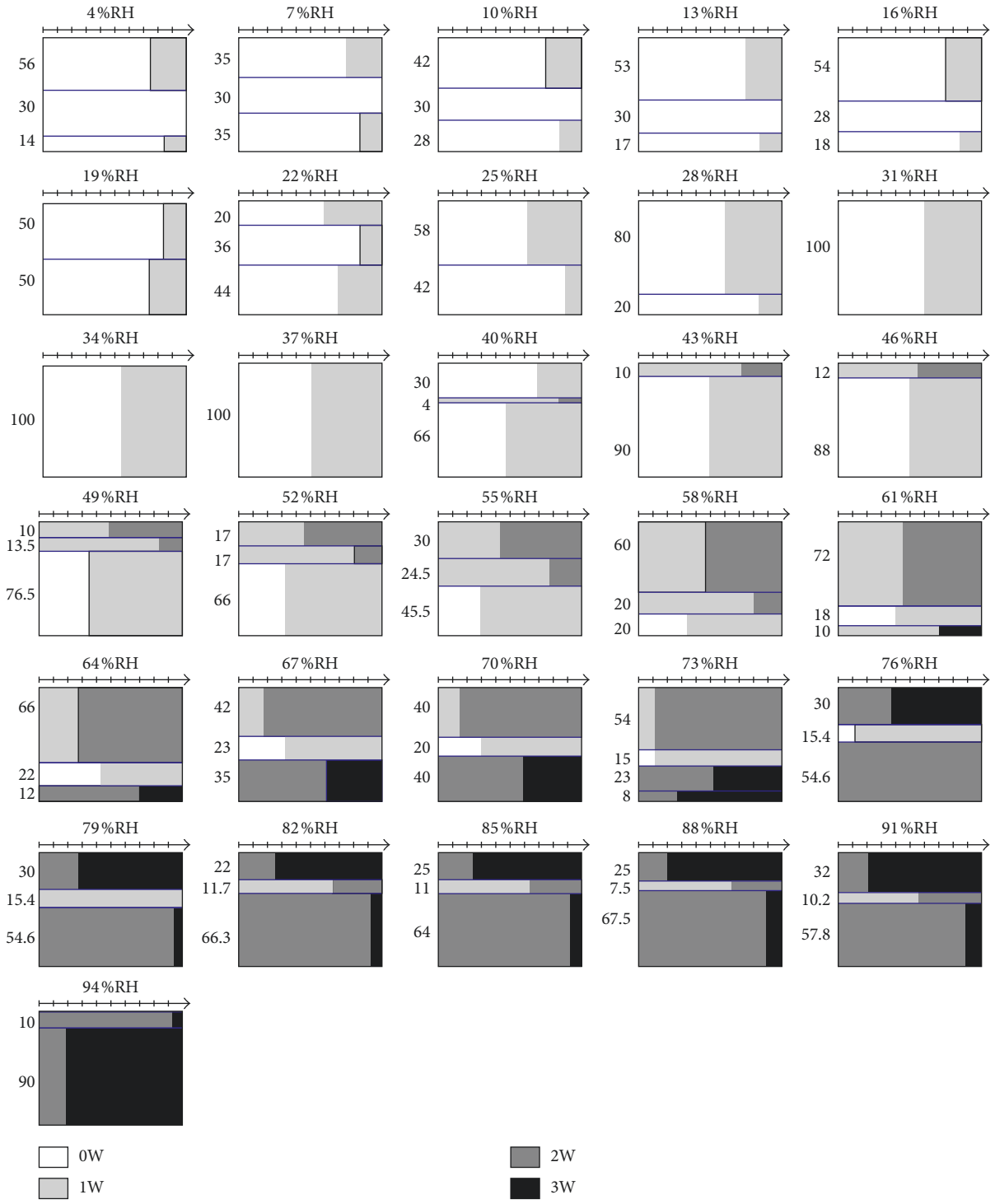

Figure 6: Schematic representation of the MLS used to fit the experimental XRD pattern in the case of the stressed sample along the sorption process.

contradicts with the qualitative analysis which assumes a homogeneous 2W phase starting at 79 %RH and ending at 64 %RH. From 70 %RH, the 1W phase is introduced in the MLS, and up to 52 %RH, the structure is fully reproduced by three layer types. At 49 %RH, the transition 3W-2W is achieved and a disappearance of the 3W phase is noted. The system is modeled using random distribution of 1W and 2W phases up to 46 %RH. The 0W phase is introduced, with minor proportions, in the MLS from 43 %RH and continues its progression in terms of abundance up to 4 %RH. At 25 %RH, the total disappearance of the 2W phase indicates the end of the 2W-1W transition.

The proposed MLS raises the ambiguity of the 3W-2W, 2W-1W, and 1W-0W transition zone limits, observed

Table 4: Some structural parameters obtained from the quantitative XRD analysis in the case of the stressed sample along the desorption process.

%RH	Layer stacking mode	M
94	R1 ($P_{AA} = 0.86$) R1 ($P_{AA} = 0.90$)	6
91	R1 ($P_{AA} = 0.90$) R1 ($P_{AA} = 0.90$)	6
88	R1 ($P_{AA} = 0.75$) R1 ($P_{AA} = 0.90$)	5
85	R0 R1 ($P_{AA} = 0.86$)	5
82	R0 R1 ($P_{AA} = 0.86$)	5
79	— R1 ($P_{AA} = 0.75$)	5
76	— R1 ($P_{AA} = 0.75$)	5
73	— R1 ($P_{AA} = 0.75$)	5
70	R0 R1 ($P_{AA} = 0.75$)	5
67	R0 R1 ($P_{AA} = 0.75$)	5
64	R0 R0 R1 ($P_{AA} = 0.75$)	5
61	R0 R0 R1 ($P_{AA} = 0.75$)	5
58	R1 ($P_{AA} = 0.95$) R1 ($P_{AA} = 0.90$) R1 ($P_{AA} = 0.75$)	5
55	R1 ($P_{AA} = 0.95$) R1 ($P_{AA} = 0.90$) R1 ($P_{AA} = 0.75$)	5
52	R1 ($P_{AA} = 0.75$) R0 R1 ($P_{AA} = 0.75$)	5
49	R1 ($P_{AA} = 0.75$) —	5
46	R1 ($P_{AA} = 0.70$) —	5
43	R1 ($P_{AA} = 0.75$) R1 ($P_{AA} = 0.92$)	5
40	R1 ($P_{AA} = 0.75$) R1 ($P_{AA} = 0.92$)	6
37	R1 ($P_{AA} = 0.75$) R1 ($P_{AA} = 0.90$)	5
34	R1 ($P_{AA} = 0.75$) R1 ($P_{AA} = 0.90$)	5
31	R1 ($P_{AA} = 0.87$) R1 ($P_{AA} = 0.90$)	5
28	R1 ($P_{AA} = 0.87$) R0	5
25	R1 ($P_{AA} = 0.79$) R1 ($P_{AA} = 0.90$)	5
22	R1 ($P_{AA} = 0.79$) R1 ($P_{AA} = 0.90$)	6
19	R1 ($P_{AA} = 0.79$) R1 ($P_{AA} = 0.85$)	6
16	R1 ($P_{AA} = 0.90$) R1 ($P_{AA} = 0.87$)	6
13	R1 ($P_{AA} = 0.95$) R1 ($P_{AA} = 0.87$)	5
10	R0 — R0	5
7	R1 ($P_{AA} = 0.55$) — R0 ($P_{AA} = 0.75$)	7
4	— R1 ($P_{AA} = 0.75$)	7

during the qualitative analysis, and precisely determines the boundaries of these transitions, despite the existing overlaps. Indeed, transition zones are characterized by asymmetry in the shape of characteristic reflections and irrational positions, and modeling has allowed a more in-depth description of hydration heterogeneities linked to these zones. The absence of a clean transition zone has been shown whatever being the RH value.

During the desorption process, the 2W phase persists up to 25 %RH, and the 1W phase endures even at 4 %RH, indicating probably the hard water molecule release mechanism for the "stressed" sample. This behavior results from the effect of the applied constraint.

4. Discussion

4.1. Water Molecule Distribution and IS Configuration. During the sorption/desorption cycle, the correlation of the results from the qualitative and quantitative XRD analyses allowed us to quantify, with precision, the composition of the clay particle studied and the contents of the IS of each type of layer. The observed fluctuations of the d_{001} basal spacing as a function of %RH are related to the variation of the water molecule amounts present in the IS.

The coexistence of different hydration states, which is an omnipresent character regardless of the constraint, is probably due to a complex insertion/release water molecule mechanism. This process remains unexplored with conventional analysis methods. The results, obtained from XRD modeling, can provide answers on the evolution of the interlamellar water abundances and their organization inducing an adequate description of the evolution of the layer thickness, according to the variation of the surrounding humidity. The evolution of the theoretical water molecules (n_{H_2O}) abundance (Figure 8), resulting from the different layer-type populations versus %RH, for the unstressed and stressed samples takes the form of a hydration hysteresis. This behavior is consistent with the results obtained by Oueslati et al. [30], who demonstrate the hysteresis material response, after external solicitation. The obtained hysteresis can be divided into three main sections, respectively, I, II, and III, as a function of the value of %RH. In fact, section I starts at 4 %RH and finishes at 37 %RH, section II is spread over the 40%–82 %RH range, and finally, section III starts at 85 %RH and ends at 94 %RH.

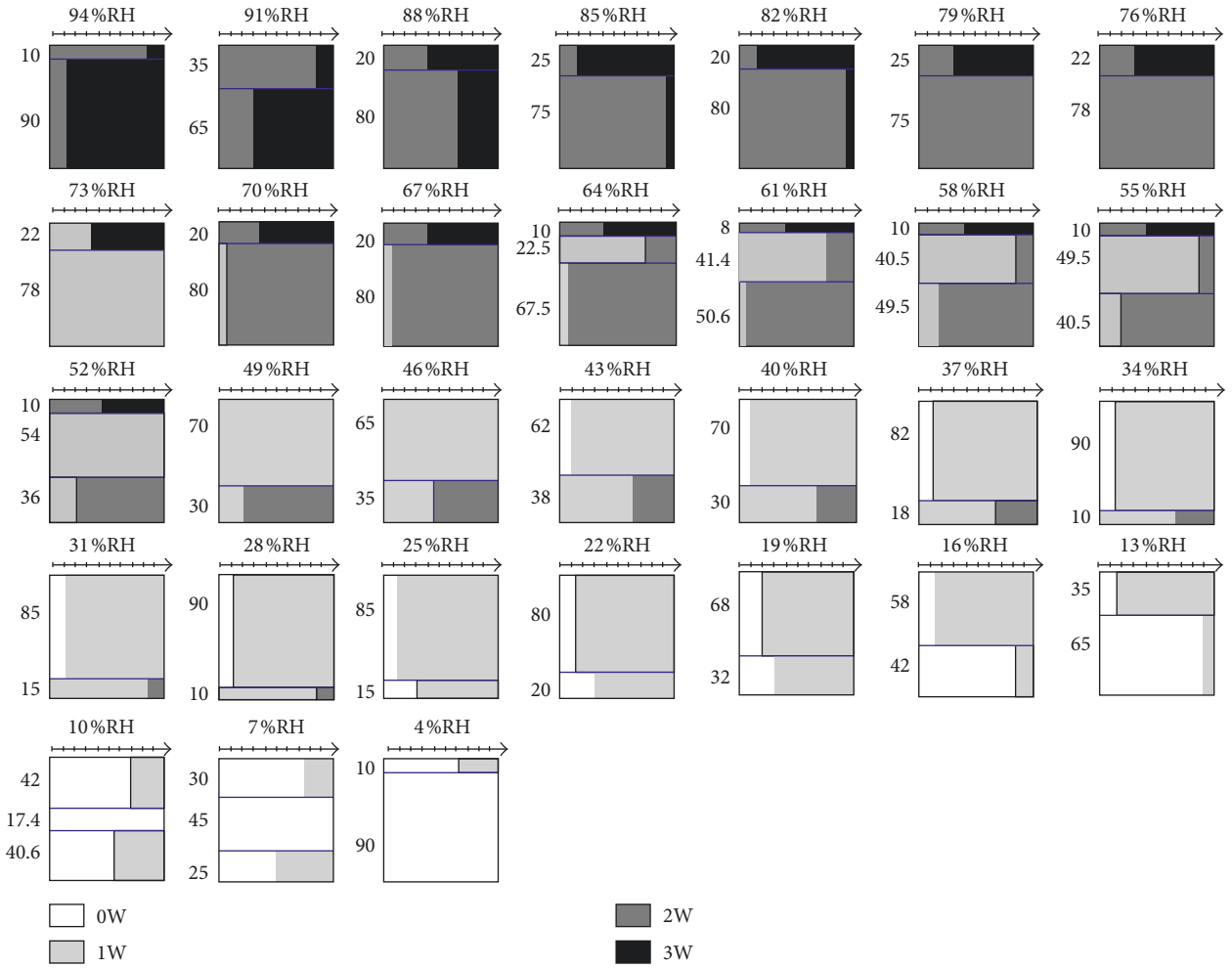

Figure 7: Schematic representation of the MLS used to fit the experimental XRD pattern in the case of the stressed sample along the desorption process.

4.1.1. Section I. For the low %RH value and until 37 %RH, a same evolution of the water molecule amount, for the unstressed and stressed samples, is noted and the variation of the environmental constraint (i.e., 50 drying/wetting cycles) does not affect the water retention mechanism. Quantitatively, this domain is totally described, at maximum, by 1W phases which are characterized by a relatively small layer thickness and a quite limited interlayer water amount. This condition imposes a restricted geometrical configuration of the IS (exchangeable cation + one water sheet) inducing a minimum freedom degree.

4.1.2. Section II. Within this section, there is a maximum water amount fluctuation and the sample has a high sensitivity to the applied atmospheric stress. Indeed, the decrease in the hysteresis thickness, for the stressed sample, indicates a significant variation in the water loss process as a function of %RH during the desorption sequence. This section can be divided in two specific phases, mentioned, respectively, (1) and (2), in blue in Figure 8. The difference between the two phases appears essentially on the curves relating to the desorption sequence.

For the phase (1), the starting sample is characterized by a hydration level with an average of $n_{H_2O} > 6$, whereas the stressed sample has a pseudolevel at $n_{H_2O} = 5.2$. In addition, the bearing relative to the starting sample is spread over a wide humidity range from 82 %RH to 55 %RH (~27%), which is not the case for the stressed sample with a fairly narrow range from 82 %RH to 67 %RH (~15%).

For the phase (2), there is a gradual and continuous decay for both samples but still keeping the offset in the number of water molecules. This behavior can be interpreted by the hypothesis of the transformation of a fraction of the "free" IS water into "structural" water, under the effect of the drying/wetting constraint, inducing a reduction in the number of vacant sites on the internal surfaces of the tetrahedral sheet and necessarily a decrease in the number of inserted water molecules. At the macroscopic scale, this means that, in the case of the "unstressed" sample, a water retention capacity is higher than that of the "stressed" one.

4.1.3. Section III. From 85% towards 94 %RH, a maximum water molecule abundance is reached and the same hydration/dehydration way is observed for the two studied

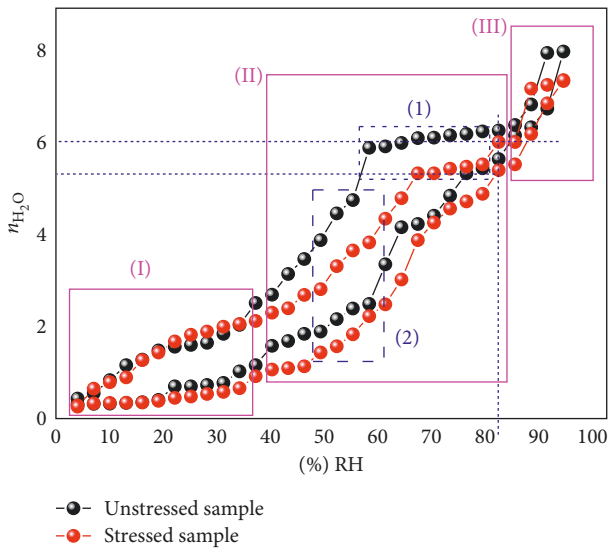

FIGURE 8: Evolution of the water molecule amounts (n_{H_2O}) versus %RH. The bottom black curve represents the sorption process of the unstressed sample. The red curve at the bottom represents the sorption process of the stressed sample. For (1) and (2) in blue, see text.

samples. This can be explained by the same principle as for Section I. Indeed, at the 3W layers hydration state, the interlamellar space is completely saturated by the geometric arrangement of the water sheets and the exchangeable cations. The stereographic configuration and the condition imposed by the physical interactions that govern the nature and arrangement of the chemical species present a constraint which limits the hydration behavior changes despite the external applied atmospheric constraint.

4.2. Hydration State Discretization. The ability of smectites to incorporate interlayer H_2O molecules and the subsequent change in d_{00l} have been studied for several decades. These observations suggested several possible models where crystalline swelling is controlled by the balance between the repulsive force owing to 2 : 1 layer interactions and the attractive forces between hydrated interlayer cations and the negatively charged surface of siloxane layers [43–46]. Few studies have taken into account the coexistence of different hydration states using the XRD profile modeling approach (with 0 to 3 planes of interlayer H_2O molecules) [47–50]. More recently, the studies [51, 52] refined this approach by fitting the 00*l* reflections over a large angular range and showed that randomly interstratified structures, each containing different layer types, coexisted in their montmorillonite samples. Ferrage et al. [24] investigate the distribution of interlayer water in bihydrated smectite from X-ray diffraction profile modeling of 00*l* reflections where they propose a new configuration for the interlayer structure of bihydrated smectite. They focused on the montmorillonite hydration properties by modeling experimental X-ray diffraction patterns recorded under controlled relative humidity (RH) conditions. Indeed, the humidity rate varies with an increment of ~20%, and it is an understandable view that the purpose of the work was to study the hydration heterogeneities in the case of several exchangeable cations. They show the systematic coexistence of smectite layer types exhibiting contrasting hydration states and a heterogeneous character for smectite hydration. This heterogeneity is characterized qualitatively using the fluctuation of FWHM and (ξ) parameters. This rule is used after that in [29, 30] to define hydration heterogeneities. Several rules deduced from the work of [25] are respected in this paper, and some results related to structural parameters such as position and amounts of exchangeable cations and the use of the MLS are in perfect concordance.

This work focuses on the discretization of the water retention mechanism, using the XRD profile modeling approach, when an external hydrous strain is applied in the case of Na-montmorillonite. The choice of the external environmental constraint (i.e., 50 drying/wetting cycles), the relative humidity variation steps (~3 %RH), and the realized limit of the extreme conditions (i.e., from 4 %RH to 94 %RH) make this work a fundamental study in order to understand the interlamellar water amount fluctuation. Indeed, the localization of the hydration transition region is accurately defined, and the hydration heterogeneities, related to the presence of more than one layer type, can be quantitatively explained. Among the strong keys of this work is the overall characterization of the abundance limits, of the dehydrated phases (0W) and the extremely hydrated phases (3W), along the sorption/desorption sequence. Indeed, after 50 drying/wetting cycles, the dehydrated and the extremely hydrated phases are more present in the stressed sample than the host material (Figure 9).

This configuration is probably due to a chemical and electrostatic equilibrium change in the interlamellar space. This change is explained by a possible adjust in the internal surface of the interlayer space following sorption/desorption cycles. Subsequent to the excessive repetition of the insertion/release water process in the starting materials, a water molecule residue has been incorporated in the internal structure which subsequently reduces the vacant site proportion inside the interlamellar space and affects its initial "function" after that (i.e., the cation exchange capacity (CEC)). By examining the evolution of the 1W and 2W abundances (Figure 9) versus %RH, a similar variation is observed for the stressed and the unstressed samples.

It remains to note that the 1W phase never reached the maximum abundance in the case of the stressed and unstressed samples. However, the 1W phase is the layer type mostly present along all the relative humidity scales. This result is interpreted by the transitional character of the 1W hydration state explained by a structural interlamellar space change with a permanent presence of the interlamellar water molecules regardless of %RH rates. The 1W phase can be considered as a transitional hydration state support. In terms of heterogeneities, a trend towards homogeneity is noted for both hysteresis terminals, whereas a heterogeneity tendency is noted for the transitional areas.

5. Conclusion

The XRD profile modeling of the 00*l* reflections allowed us to characterize the structural changes along the c^* axis of the

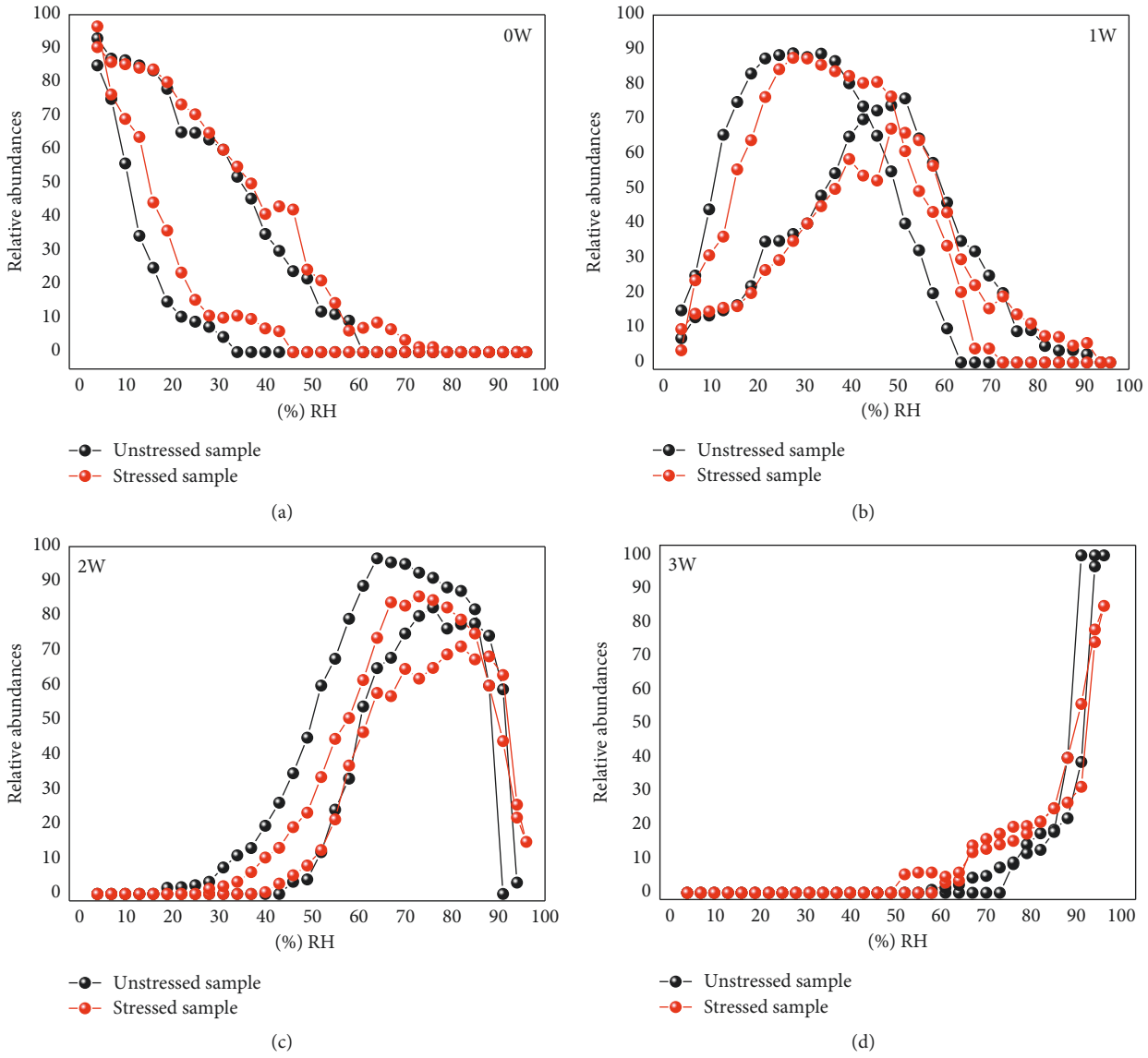

FIGURE 9: Evolution of the individual relative abundance of each hydration state as a function of the relative humidity (%RH) in the case of unstressed and stressed samples.

SWy-2-Na sample before and after application of the atmospheric stress. The obtained results are as follows:

(i) A new hydration behavior of the "stressed" sample described by fluctuations in the hydration hysteresis as a function of the RH rates.

(ii) The application of the sorption/desorption process by "in situ" variation of the %RH, before and after applying the constraint, made it possible to identify the homogeneous hydration states and the hydration transition zones, which are characterized by a high heterogeneity degree.

(iii) Structural heterogeneities are characterized by an elevated MLS number. Indeed, two possible configurations of IS contents, 0W/1W/2W and 1W/2W/3W, with variable relative abundances, are discerned over a wide explored RH range.

(iv) Iteration of the insertion/release phenomenon of the water molecules, during drying/wetting cycles, induces an increase in the relative abundance of the 0W and 3W population at the expense of the abundances of the 1W and 2W phases. This result explains the limits observed during the sorption/desorption process in the case of the stressed sample.

Conflicts of Interest

The authors declare that they have no conflicts of interest.

Acknowledgments

The authors specially thank Bruno Lanson (ISTerre, Grenoble, France) for his availability, his fruitful discussions on the XRD modeling approach, and his advice on the work

presentation. The authors also thank Nathaniel Findling (ISTerre, Grenoble, France) for the assistance during XRD and sorption/desorption data collection.

Supplementary Materials

Figure S1: best agreement obtained between experimental (black) and modeled (red) XRD patterns in the case of the SWy-2-Na sample versus %RH. The sorption sequence by increasing %RH: 4–25 %RH (a), 28–49 %RH (b), 52–73 %RH (c), and 76–94 %RH (d). For all XRD patterns, the intensity is arbitrary. The theoretical decomposition of the experimental patterns (blue, red, and green) is on the left. The obtained best agreement is on the right. For each %RH value, the 001 line is recorded twice (in black) in order to check the sample balance with its environment. *Halite (NaCl) complex. Figure S2: best agreement obtained between experimental (black) and modeled (red) XRD patterns in the case of the SWy-2-Na sample versus %RH. The desorption sequence by decreasing %RH: 94–70 %RH (a), 67–46 %RH (b), 43–25 %RH (c), and 22–4 %RH (d). For all XRD patterns, the intensity is arbitrary. The theoretical decomposition of the experimental patterns (blue, red, and green) is on the left. The final best agreement is on the right. *Halite (NaCl) complex. Figure S3: best agreement obtained between experimental (black) and modeled (red) XRD patterns in the case of the stressed sample versus %RH. The sorption sequence obtained by increasing %RH: 4–25 %RH (a), 28–46 %RH (b), 49–70 %RH (c), and 73–94 %RH (d). For all XRD patterns, the intensity is arbitrary. The theoretical decomposition of the experimental patterns (blue, red, and green) is on the left. The obtained best agreement is on the right. *Halite (NaCl) complex. Figure S4: best agreement obtained between experimental (black) and modeled (red) XRD patterns in the case of the stressed sample versus %RH. The desorption sequence obtained by increasing %RH: 4–25 %RH (a), 28–46 %RH (b), 49–70 %RH (c), and 73–94 %RH (d). For all XRD patterns, the intensity is arbitrary. The theoretical decomposition of the experimental patterns (blue, red, and green) is on the left. The obtained best agreement is on the right. *Halite (NaCl) complex. (*Supplementary Materials*)

References

[1] H.-J. Herbert, J. Kasbohm, H. Sprenger, A. M. Fernández, and C. Reichelt, "Swelling pressures of MX-80 bentonite in solutions of different ionic strength," *Physics and Chemistry of the Earth, Parts A/B/C*, vol. 33, no. S1, pp. S327–S342, 2008.

[2] T. Higashihara, K. Kinoshita, Y. Akagi, S. Sato, and T. Kozaki, "Transport number of sodium ions in water-saturated, compacted Na-montmorillonite," *Physics and Chemistry of the Earth, Parts A/B/C*, vol. 33, no. S1, pp. S142–S148, 2008.

[3] M. V. Villara, M. Sánchez, and A. Gens, "Behaviour of a bentonite barrier in the laboratory: experimental results up to 8 years and numerical simulation," *Physics and Chemistry of the Earth, Parts A/B/C*, vol. 33, no. S1, pp. S476–S485, 2008.

[4] T. Kozaki, J. Liua, and S. Sato, "Diffusion mechanism of sodium ions in compacted montmorillonite under different NaCl concentration," *Physics and Chemistry of the Earth, Parts A/B/C*, vol. 33, no. 14–16, pp. 957–961, 2008.

[5] T. Kozaki, T. Sawaguchi, A. Fujishima, and S. Sato, "Effect of exchangeable cations on apparent diffusion of Ca2+ ions in Na- and Ca-montmorillonite mixtures," *Physics and Chemistry of the Earth, Parts A/B/C,*vol. 35, no. 6–8, pp. 254–258, 2010.

[6] O. Karnland, M. Birgersson, and M. Hedström, "Selectivity coefficient for Ca/Na ion exchange in highly compacted bentonite," *Physics and Chemistry of the Earth, Parts A/B/C*, vol. 36, no. 17–18, pp. 1554–1558, 2011.

[7] K. K. Norrfors, M. Bouby, S. Heck et al., "Montmorillonite colloids: I. Characterization and stability of dispersions with different size fractions," *Applied Clay Science*, vol. 114, pp. 179–189, 2015.

[8] W. F. Bradley, R. E. Grim, and G. F. Clark, "A study of the behavior of montmorillonite on wetting," *Zeitschrift Kristallographie*, vol. 97, pp. 260–270, 1937.

[9] J. Méring and R. Glaeser, "Sur le rôle de la valence des cations échangeables dans la montmorillonite," *Bulletin de la Société Francaise de Minéralogie et Cristallographie*, vol. 77, pp. 519–530, 1954.

[10] S. Dultz, J.-H. An, and B. Riebe, "Organic cation exchanged montmorillonite and vermiculite as adsorbents for Cr(VI): effect of layer charge on adsorption properties," *Applied Clay Science*, vol. 67-68, pp. 125–133, 2012.

[11] D. M. Moore and R. C. Reynolds Jr., *X-Ray Diffraction and the Identification and Analysis of Clay Minerals*, Oxford University Press, New York, NY, USA, 1997.

[12] B. Dazas, B. Lanson, J. Breu, J.-L. Robert, M. Pelletier, and E. Ferrage, "Smectite fluorination and its impact on interlayer water content and structure: a way to fine tune the hydrophilicity of clay surfaces?," *Microporous and Mesoporous Materials*, vol. 181, pp. 233–247, 2013.

[13] A. Kaya and H. Y. Fang, "The effects of organic fluids on physicochemical parameters of fine-grained soils," *Canadian Geotechnical Journal*, vol. 37, no. 5, pp. 943–950, 2000.

[14] M. H. Fu, Z. Z. Zhang, and P. F. Low, "Changes in the properties of a montmorillonite-water system during the adsorption and desorption of water: hysteresis," *Clays and Clay Minerals*, vol. 38, pp. 485–492, 1990.

[15] E. S. Boek, P. V. Coveney, and N. T. Skipper, "Monte Carlo molecular modeling studies of hydrated Li-, Na-, and K-smectites: understanding the role of potassium as a clay swelling inhibitor," *Journal of the American Chemical Society*, vol. 117, no. 50, pp. 12608–12617, 1995.

[16] E. S. Boek, P. V. Coveney, and N. T. Skipper, "Molecular modeling of clay hydration: a study of hysteresis loops in the swelling curves of sodium montmorillonites," *Langmuir*, vol. 11, no. 12, pp. 4629–4631, 1995.

[17] F.-R. C. Chang, N. T. Skipper, and G. Sposito, "Computer simulation of interlayer molecular structure in sodium montmorillonite hydrates," *Langmuir*, vol. 11, no. 7, pp. 2734–2741, 1995.

[18] F.-R. C. Chang, N. T. Skipper, and G. Sposito, "Monte Carlo and molecular dynamics simulations of interfacial structure in lithium-montmorillonite hydrates," *Langmuir*, vol. 13, no. 7, pp. 2074–2082, 1997.

[19] N. T. Skipper, F. R. C. Chang, and G. Sposito, "Monte Carlo simulation of interlayer molecular structure in swelling clay minerals. 1. Methodology," *Clays and Clay Minerals*, vol. 43, no. 3, pp. 285–293, 1995.

[20] S. Karaborni, B. Smit, W. Heidug, J. Urai, and E. van Oort, "The swelling of clays: molecular simulations of the hydration of montmorillonite," *Science*, vol. 271, no. 5252, pp. 1102–1104, 1996.

[21] Q. H. Zeng, A. B. Yu, G. Q. Lu, and R. K. Standish, "Molecular dynamics simulation of the structural and dynamic properties of dioctadecyldimethyl ammoniums in organoclays," *Journal of Physical Chemistry B*, vol. 108, no. 28, pp. 10025–10033, 2004.

[22] A. Meleshyn and C. Bunnenberg, "Swelling of Na/Mg-montmorillonites and hydration of interlayer cations: a Monte Carlo study," *Journal of Chemical Physics*, vol. 123, no. 7, article 074706, 2005.

[23] D. E. Smith, Y. Wang, A. Chaturvedi, and H. D. Whitley, "Molecular simulations of the pressure, temperature, and chemical potential dependencies of clay swelling," *Journal of Physical Chemistry B*, vol. 110, no. 40, pp. 20046–20054, 2006.

[24] E. Ferrage, B. Lanson, B. A. Sakharov, and V. A. Drits, "Investigation of smectite hydration properties by modeling of X-ray diffraction profiles. Part 1. Montmorillonite hydration properties," *American Mineralogist*, vol. 90, no. 8-9, pp. 1358–1374, 2005.

[25] E. Ferrage, B. Lanson, N. Malikova, A. Plançon, B. A. Sakharov, and V. A. Drits, "New insights on the distribution of interlayer H_2O molecules in bi-hydrated smectite from X-ray diffraction profile modeling of 00l reflections," *Chemistry of Materials*, vol. 17, no. 13, pp. 3499–3512, 2005.

[26] E. Ferrage, B. Lanson, B. A. Sakharov, N. Geoffroy, E. Jacquot, and V. A. Drits, "Investigation of smectite hydration properties by modeling of X-ray diffraction profiles. Part 2. Influence of layer charge and charge location," *American Mineralogist*, vol. 92, no. 10, pp. 1731–1743, 2007.

[27] W. Oueslati, M. S. Karmous, H. Ben Rhaiem, B. Lanson, and A. Ben Haj Amara, "Effect of interlayer cation and relative humidity on the hydration properties of a dioctahedral smectite," *Zeitschrift für Kristallographie Supplements*, vol. S26, pp. 417–422, 2007.

[28] W. Oueslati, H. B. Rhaiem, B. Lanson, and A. B. H. Amara, "Selectivity of Na–montmorillonite in relation with the concentration of bivalent cation (Cu^{2+}, Ca^{2+}, Ni^{2+}) by quantitative analysis of XRD patterns," *Applied Clay Science*, vol. 43, no. 2, pp. 224–227, 2009.

[29] W. Oueslati, H. Ben Rhaiem, and A. Ben Haj Amara, "XRD investigations of hydrated homoionic montmorillonite saturated by several heavy metal cations," *Desalination*, vol. 271, no. 1–3, pp. 139–149, 2011.

[30] W. Oueslati, H. Ben Rhaiem, and A. Ben Haj Amara, "Effect of relative humidity constraint on the metal exchanged montmorillonite performance: an XRD profile modeling approach," *Applied Surface Science*, vol. 261, pp. 396–404, 2012.

[31] B. Dazas, E. Ferrage, A. Delville, and B. Lanson, "Interlayer structure model of tri-hydrated low-charge smectite by X-ray diffraction and Monte Carlo modeling in the Grand Canonical ensemble," *American Mineralogist*, vol. 99, no. 8-9, pp. 1724–1735, 2014.

[32] T. Sato, T. Watanabe, and R. Otsuka, "Effects of layer charge, charge location, and energy change on expansion properties of dioctahedral smectites," *Clays and Clay Minerals*, vol. 40, no. 1, pp. 103–113, 1992.

[33] W. Oueslati, M. Ammar, and N. Chorfi, "Quantitative XRD analysis of the structural changes of Ba-exchanged montmorillonite: effect of an in situ hydrous perturbation," *Minerals*, vol. 5, no. 3, pp. 507–526, 2015.

[34] W. F. Moll, "Baseline studies of the Clay Minerals Society Source Clays: geological origin," *Clays and Clay Minerals*, vol. 49, no. 5, pp. 374–380, 2001.

[35] A. R. Mermut and A. F. Cano, "Baseline studies of the Clay Minerals Society Source Clays: chemical analyses of major elements," *Clays and Clay Minerals*, vol. 49, no. 5, pp. 381–386, 2001.

[36] J. L. Post, B. L. Cupp, and F. T. Madsen, "Beidellite and associated clays from the DeLamar Mine and Florida Mountain area, Idaho," *Clays and Clay Minerals*, vol. 45, no. 2, pp. 240–250, 1997.

[37] D. Tessier, "Experimental study of the clay materials organization. Hydration, swelling and structure along drying and re-wetting," Thesis, University of Paris VII, Publication INRA Versailles, Paris, France, 1984.

[38] S. W. Bailey, "Nomenclature for regular interstratifications," *American Mineralogist*, vol. 67, pp. 394–398, 1982.

[39] M. Ammar, W. Oueslati, H. B. Rhaiem, and A. B. H. Amara, "Quantitative XRD analysis of the dehydration–hydration performance of (Na^+, Cs^+) exchanged smectite," *Desalination and Water Treatment*, vol. 52, no. 22–24, pp. 4314–4333, 2014.

[40] M. Ammar, W. Oueslati, H. B. Rhaiem, and A. B. H. Amara, "Effect of the hydration sequence orientation on the structural properties of Hg exchanged montmorillonite: quantitative XRD analysis," *Journal of Environmental Chemical Engineering*, vol. 2, no. 3, pp. 1604–1611, 2014.

[41] V. A. Drits and C. Tchoubar, *X-ray Diffraction by Disordered Lamellar Structures: Theory and Applications to Microdivided Silicates and Carbons*, Springer, Berlin, Germany, 1990.

[42] B. A. Sakharov and B. Lanson, "X-ray identification of mixed-layer structures. Modelling of diffraction effects," in *Handbook of Clay Science*, F. Bergaya and G. Lagaly, Eds., vol. 5B, pp. 51–135, Elsevier, Amsterdam, Netherlands, 2013.

[43] K. Norrish, "The swelling of montmorillonite," *Discussions of the Faraday Society*, vol. 18, pp. 120–133, 1954.

[44] H. van Olphen, "Thermodynamics of interlayer adsorption of water in clays," *Journal of Colloid Science*, vol. 20, no. 8, pp. 822–837, 1965.

[45] D. A. Laird, "Influence of layer charge on swelling of smectites," *Applied Clay Science*, vol. 34, no. 1–4, pp. 74–87, 2006.

[46] B. Lanson, "Modelling of X-ray diffraction profiles: investigation of defective lamellar structure crystal chemistry,"*EMU Notes in Mineralogy*, Chapter 4, vol. 11, pp. 151–202, Mineralogical Society Great Britain & Ireland, Ireland, 2011.

[47] T. Iwasaki and T. Watanabe, "Distribution of Ca and Na ions in dioctahedral smectites and interstratified dioctahedral mica/smectites," *Clays and Clay Minerals*, vol. 36, no. 1, pp. 73–82, 1988.

[48] I. Bérend, J. M. Cases, M. François et al., "Mechanism of adsorption and desorption of water vapour by homoionic montmorillonites: 2. The Li^+, Na^+, K^+, Rb^+ and Cs^+ exchanged forms," *Clays and Clay Minerals*, vol. 43, no. 3, pp. 324–336, 1995.

[49] J. M. Cases, I. Bérend, M. François, J. P. Uriot, L. J. Michot, and F. Thomas, "Mechanism of adsorption and desorption of water vapour by homoionic montmorillonite: The Mg^{2+}, Ca^{2+}, Sr^{2+} and Ba^{2+} exchanged forms," *Clays and Clay Minerals*, vol. 45, no. 1, pp. 8–22, 1997.

[50] J. Cuadros, "Interlayer cation effects on the hydration state of smectite," *American Journal of Science*, vol. 297, no. 8, pp. 829–841, 1997.

[51] L. Calarge, B. Lanson, A. Meunier, and M. L. Formoso, "The smectitic minerals in a bentonite deposit from Melo (Uruguay)," *Clay Minerals*, vol. 38, no. 1, pp. 25–34, 2003.

[52] A. Meunier, B. Lanson, and B. Velde, "Composition variation of illite-vermiculite-smectite mixed-layer minerals in a bentonite bed from Charente (France)," *Clay Minerals*, vol. 39, no. 3, pp. 187–196, 2004.